

# Foaming Species and Trapping Mechanisms in Barium Silicate Glass Sealants

Ralf Müller,\* Harald Behrens, Boris Agea-Blanco, Stefan Reinsch, and Thomas Wirth

Barium silicate glass powders 4 h milled in CO<sub>2</sub> and Ar and sintered in air are studied with microscopy, total carbon analysis, differential thermal analysis (DTA), vacuum hot extraction mass spectroscopy (VHE-MS), Fourier-transformed infrared (FTIR) spectroscopy, X-ray photoelectron spectroscopy (XPS), and time-of-flight secondary-ion mass spectrometry (TOF-SIMS). Intensive foaming of powder compacts is evident, and VHE studies prove that foaming is predominantly caused by carbonaceous species for both milling gases. DTA shows that the decomposition of BaCO<sub>3</sub> particles mix-milled with glass powders occurs at similar temperatures as foaming of compacts. However, no carbonate at the glass surface could be detected by FTIR spectroscopy, XPS, and TOF-SIMS after heating to the temperature of sintering. Instead, CO<sub>2</sub> molecules unable to rotate identified by FTIR spectroscopy after milling, probably trapped by mechanical dissolution into the glass bulk. Such a mechanism or microencapsulation in cracks and particle aggregates can explain the contribution of Ar to foaming after intense milling in Ar atmosphere. The amount of CO<sub>2</sub> molecules and Ar, however, cannot fully explain the extent of foaming. Carbonates mechanically dissolved beneath the surface or encapsulated in cracks and micropores of particle aggregates are therefore probably the major foaming source.

Due to the low viscosity required for joining and gas tight sealing, gas bubble formation and subsequent swelling (foaming) often occur, even when organic acids are not used in powder processing. In contrast to the extensive and ongoing study of desired foaming phenomena utilized for foam glasses or glass-ceramic foams,<sup>[9–15]</sup> this undesired foaming effect and its underlying mechanisms are rarely reported. Lucchini<sup>[16]</sup> observed bubble formation for sodium and calcium lead silicate glass-bonded barium hexaferrites and discussed glass volatilization as the underlying mechanism. Pore formation was also found in porcelain stoneware tiles<sup>[17]</sup> and lead borosilicate glass frits,<sup>[18]</sup> where effusing oxygen or water, physically or chemically adsorbed to the powder surface, was discussed as the foaming source. Lara et al.<sup>[19]</sup> reported foaming during the sintering and crystallization of Ca, Mg, and Zn aluminosilicate glass powders used for solid oxide fuel cell (SOFC) sealing. The authors believed that density changes or gas evolution

## 1. Introduction

Glass powders are widely used in fabricating sintered glasses, sintered glass-ceramics, glass matrix composites, seals, and glass-bonded ceramics or pastes.<sup>[1–3]</sup> For many of these applications, glasses with low crystallization tendency are used, for example, for low-temperature cofired ceramics,<sup>[4,5]</sup> pastes,<sup>[6]</sup> or sealants<sup>[7,8]</sup> to ensure sufficient sinterability.


tion during crystallization are responsible for foaming. Undesired porosity was also reported to occur during sintering of BaO-B<sub>2</sub>O<sub>3</sub>-SiO<sub>2</sub>,<sup>[20]</sup> lead-free Bi<sub>2</sub>O<sub>3</sub>-B<sub>2</sub>O<sub>3</sub>-SiO<sub>2</sub> solder glass,<sup>[21]</sup> LTCC glass powders,<sup>[22]</sup> as well as during porcelain tiles production.<sup>[23]</sup>

More recently, Agea-Blanco et al.<sup>[24]</sup> studied sintering and foaming of commercial barium zinc alumino boro silicate glass powders, used for SOFC sealing, with heating microscopy, differential thermal analysis (DTA), and vacuum hot extraction (VHE). It was shown that foaming intensity increases with milling duration. For moderately milled glass powders, consecutive storage in air could also promote foaming. Although powder compacts were pressed and sintered in air, foaming was affected by different milling atmospheres among which CO<sub>2</sub> proved to enhance foaming most strongly. Similarly, VHE studies revealed that foaming is predominantly driven by C, CO, and CO<sub>2</sub>, even for powders milled in Ar and N<sub>2</sub>. It was therefore concluded that foaming is caused by carbonaceous species adsorbed on the glass powder surface during milling and later storage.

The present study is focused on the nature of these species and the mechanisms keeping them trapped during heating to the temperature of foaming. To ensure detectable amounts of foaming species, K01 glass powders were milled for several hours. Recrushed powder compacts, or those heated to different temperatures and quenched in air were studied with heating

R. Müller, B. Agea-Blanco, S. Reinsch, Dr. T. Wirth  
Division 5.6 Glass  
Bundesanstalt für Materialforschung und -prüfung (BAM)  
Richard-Willstätter-Str.11, 12489 Berlin, Germany  
E-mail: ralf.mueller@bam.de

H. Behrens  
Institute of Mineralogy  
Leibniz Universität Hannover  
Callinstr. 3-9, 30167 Hannover, Germany

 The ORCID identification number(s) for the author(s) of this article can be found under <https://doi.org/10.1002/adem.202100445>.

© 2021 The Authors. Advanced Engineering Materials published by Wiley-VCH GmbH. This is an open access article under the terms of the Creative Commons Attribution License, which permits use, distribution and reproduction in any medium, provided the original work is properly cited.

DOI: 10.1002/adem.202100445

microscopy, DTA, microscopy, total carbon analysis, VHE, FTIR spectroscopy, X-ray photoelectron spectroscopy (XPS), and time-of-flight secondary-ion mass spectrometry (TOF–SIMS), to trace foaming species uptake and trapping during glass powder processing.

## 2. Results

### 2.1. Particle Size, Surface Area, and Total Carbon Content

**Table 1** shows particle size distribution parameters ( $D_{10}$ ,  $D_{50}$ ,  $D_{90}$ ), as well as measured ( $A^{\text{BET}}$ ) and estimated specific surface area values ( $A^{\text{Calc}}$ ) and the total carbon content (C) for the glass powders studied. Due to their nonspherical shape and the presence of agglomerates expected for intensive milling,  $A^{\text{BET}}$  is larger than  $A^{\text{Calc}}$ . The powder 5 min mix-milled with  $\text{BaCO}_3$  was used for measuring the decomposition temperature of mechanically damaged  $\text{BaCO}_3$  particles with DTA. The powders 1 and 4 h milled in Ar and  $\text{CO}_2$  were used for FTIR, XPS, and TOF–SIMS studies conducted to identify foaming sources. The total carbon content was particularly high in the powder obtained after milling for 4 h in  $\text{CO}_2$ . A comparison with the crushed powder gives evidence that the detected carbon does not originate from glass production. About 700 wt. ppm C were still detected in the 4 h  $\text{CO}_2$ -milled powder after heating to 710 °C, which can be either relicts surviving the heating process or carbon species adsorbed after cooling. As  $\text{CO}_2$  was basically absent during milling in Ar atmosphere; the carbon measured on the Ar-milled samples most likely is due to the adsorption of carbon species after milling.

### 2.2. Foaming

**Figure 1** shows the sintering and foaming behavior of powder compacts during heating at 5 K min<sup>-1</sup> in terms of silhouette area change,  $s_A$ , measured by heating microscopy. Intensive foaming is evident for milling in  $\text{CO}_2$ , where  $s_A$  increases to ≈380%. Although some tiny shrinking starts at ≈700 °C, the early onset of intensive foaming at ≈720 °C prevents any further shrinkage. **Figure 2** shows that a large amount of porosity evolved already at this temperature. These pores predominantly appear at the edges and in the interstices of larger glass grains, whereas their interior is still bubble free.

**Table 1.** Particle size, specific surface area, and total carbon analysis.  $D_x$  = particle diameter below which x mass% of all particles were measured.  $A^{\text{BET}}$  and  $A^{\text{Calc}}$  = specific powder surface area measured and estimated from  $D_{50}$ , assuming uniform spherical particles, respectively. C = total carbon content.

Glass powder	$D_{10}$ [μm]	$D_{50}$ [μm]	$D_{90}$ [μm]	$A^{\text{BET}}$ [m <sup>2</sup> g <sup>-1</sup> ]	$A^{\text{Calc}}$ [m <sup>2</sup> g <sup>-1</sup> ]	C [wt ppm]
Crushed in air	18.05	222.78	538.32	0.141	0.063	44
5 min milled in air	4.50	43.50	112.00	–	–	–
5 min mix-milled with $\text{BaCO}_3$ in air	0.80	3.00	31.70	–	–	–
1 h milled in $\text{CO}_2$	1.15	7.30	25.02	0.645	0.536	–
4 h milled in Ar	0.75	2.83	20.30	2.082	0.911	394
4 h milled in $\text{CO}_2$	0.81	3.12	13.77	1.441	0.859	1428
4 h milled in $\text{CO}_2$ , heated to 710 °C <sup>a)</sup>	–	–	–	–	–	700

<sup>a)</sup>Heating at 15 K min<sup>-1</sup> to 710 °C, reaching  $s_A = -4.5\%$  equal to that at the foaming onset of the 4 h  $\text{CO}_2$  milled powder shown in Figure 1.

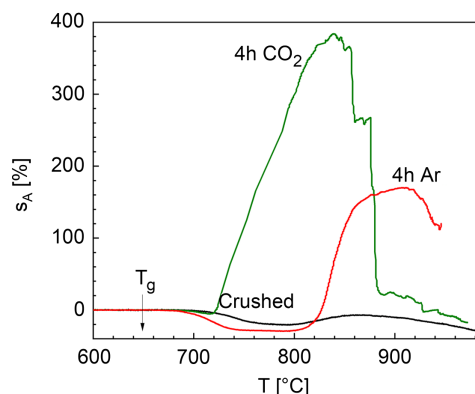


**Figure 1.** Silhouette area change,  $s_A$ , of powder compacts uniaxially pressed from glass powders 4 h milled in  $\text{CO}_2$ , 4 h milled in Ar, or crushed during heating at 5 K min<sup>-1</sup> versus temperature.

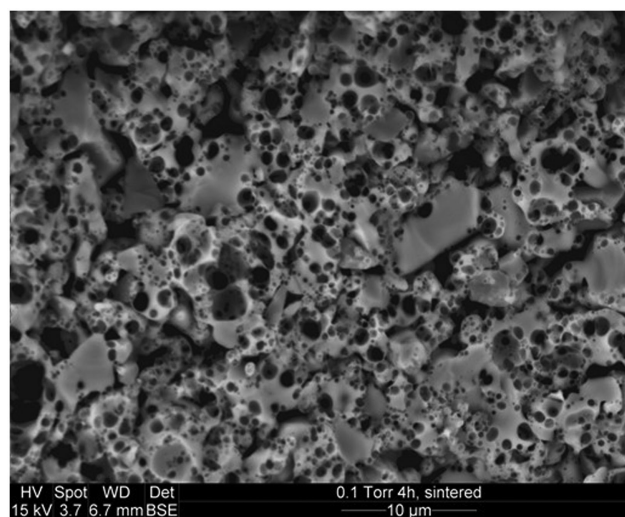


**Figure 2.** Scanning electron micrograph of a fracture surface of a compact of the glass powder milled for 4 h in  $\text{CO}_2$ . The compact was heated at 5 K min<sup>-1</sup> to 693 °C and held until reaching  $s_A = -4.5\%$  before quenching.

Sintering of the powder milled in Ar similarly starts at ≈680 °C. However, foaming occurs far above densification

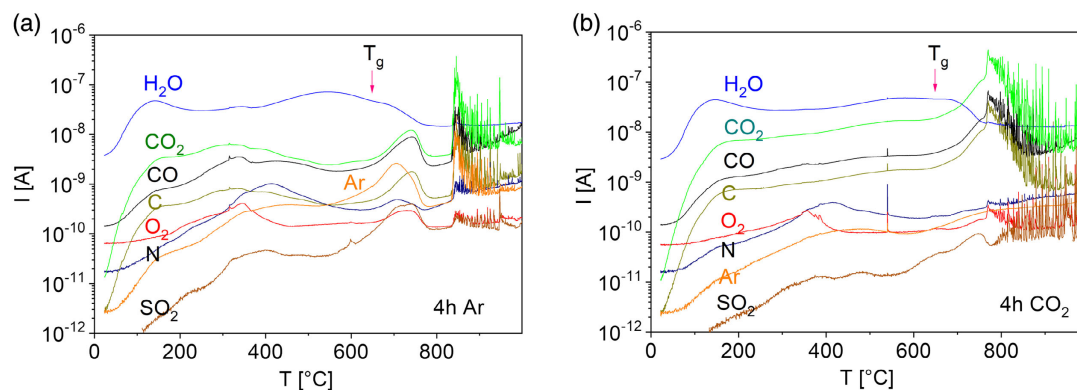


**Figure 3.** VHE degassing ion current,  $I$ , versus temperature,  $T$ , for K01 glass powders milled in a) Ar and b)  $\text{CO}_2$  during heating at  $20 \text{ K min}^{-1}$ .

and  $s_A$  less strongly increases to  $\approx 170\%$ . The increase in foaming intensity caused by milling in  $\text{CO}_2$  instead of Ar is probably even larger than that shown by Figure 1 as  $s_A$  reflects a dynamic balance between gas bubble growth and bursting. Bubble bursting  $> 800^\circ\text{C}$  is in fact indicated by the jagged  $s_A$  curve for milling in  $\text{CO}_2$  (Figure 1) and pronounced degassing spikes in **Figure 3**. The easier bursting of large gas bubbles might also explain why the compact fully collapses at lower temperature.

The strong foaming of the 4 h  $\text{CO}_2$ -milled glass powder was not further promoted by storage in ambient air for up to 125 days before uniaxial pressing. In contrast, the less strong foaming found for 4 h milling in Ar was noticeably enhanced after storage in ambient air. After 65 days storage,  $s_A$  increased to 220%, and foaming started at  $770^\circ\text{C}$ .

### 2.3. Gas Release

Figure 3 shows degassing curves of K01 glass powders milled 4 h in Ar or  $\text{CO}_2$ . For the powder milled in Ar, not only Ar but also  $\text{H}_2\text{O}$ ,  $\text{CO}_2$ , CO, C,  $\text{SO}_2$ , N, and  $\text{O}_2$  are detectable. For milling in  $\text{CO}_2$ , degassing is particularly strong for carbon-related species ( $\text{CO}_2$ , CO, C). Broad peaks between  $100^\circ\text{C}$  and  $600^\circ\text{C}$  indicate gas desorption from the glass surface.<sup>[25]</sup> Accordingly, substantial desorption of carbon-related species in this temperature range was found by DTA-MS measurements in the study by Agea-Blanco et al.<sup>[24]</sup>

For the powder 4 h milled in Ar, degassing activity newly increases above  $T_g$  ( $\approx 650^\circ\text{C}$ , arrow) for most species (except for water). Above  $740^\circ\text{C}$ , this degassing activity decreases due to sintering (Figure 1) as open porosity collapses and all diffusing species have to overcome longer distances before escaping. For 4 h milling in  $\text{CO}_2$ , however, this effect does not occur. Consistent with Figure 1, 2, and Table 1, this finding confirms that intensive degassing causes early gas bubble formation, which counteracts any detectable sinter shrinkage.

After further heating, higher species diffusivity and lower viscosity allow gas bubble growth and bursting and, this way, the volatile species temporarily entrapped during compact densification can now escape. This phenomenon is indicated by the degassing spikes in Figure 3. It should be noted that this degassing mechanism, that is, foaming, is primarily driven by carbon-related species as already reported in the study by

Agea-Blanco et al.<sup>[24]</sup>  $\text{H}_2\text{O}$  does not contribute significantly to foaming in both cases. This observation indicates that the decrease in degassing activity of water above  $T_g$  most likely reflects a depletion of  $\text{H}_2\text{O}$  rather than degassing retardation due to sintering.

### 2.4. DTA

As a possible source of foaming,  $\text{BaCO}_3$  powder was studied with DTA (**Figure 4**, dashed curve). Its decomposition occurs at  $900\text{--}1200^\circ\text{C}$ , at a much higher temperature than foaming ( $700\text{--}900^\circ\text{C}$  for milling in  $\text{CO}_2$  Figure 1). However, the decomposition temperature of  $\text{BaCO}_3$  depends on the experimental condition and the nature of the material. This is clearly illustrated by different decomposition peak temperatures reported in literature as  $\approx 840^\circ\text{C}$  for heating at  $10 \text{ K min}^{-1}$  in air,<sup>[26]</sup>  $> 850^\circ\text{C}$  for heating at  $13 \text{ K min}^{-1}$  in He,<sup>[27]</sup> and  $930\text{--}1150^\circ\text{C}$  for heating at  $2.5\text{--}10 \text{ K min}^{-1}$  in  $\text{N}_2$ .<sup>[28]</sup> To study  $\text{BaCO}_3$  decomposition at conditions as close as possible to the sintering experiments, a  $\text{BaCO}_3$  powder was 5 min mix-milled with K01 glass powder of equal mass before being studied (Figure 4, solid curve). This experiment shows that the decomposition temperature range of mechanically damaged small  $\text{BaCO}_3$  particles ( $650\text{--}900^\circ\text{C}$ ) is quite similar to the temperature

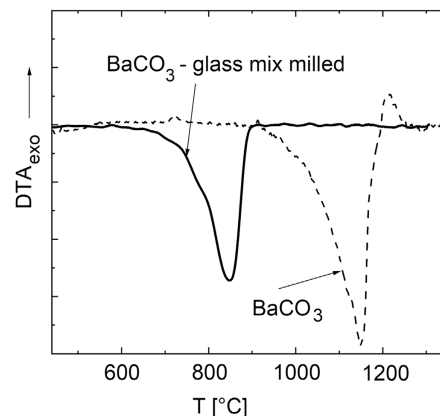


**Figure 4.** DTA curves of pure  $\text{BaCO}_3$  powder as received and  $\text{BaCO}_3$  powder 5 min mix-milled with glass powder. Heating rate was  $5 \text{ K min}^{-1}$ .

range of foaming. Thus,  $\text{BaCO}_3$  formed by glass alteration could be a possible source of foaming. However, it is not sure that our experiment adequately mimics the decomposition behavior of poorly crystallized, nanoprecipitates of  $\text{BaCO}_3$  on glass surfaces.

## 2.5. IR Spectroscopy

ATR–FTIR spectra of glass powders differently milled and heated are shown in Figure 5, which focuses on the spectral range of carbonaceous species (arrows).<sup>[29]</sup> A weak shoulder appears at  $1540\text{--}1630\text{ cm}^{-1}$ , best seen for 4 h milling in  $\text{CO}_2$ . This shoulder could be caused, for example, by asymmetric stretching vibrations of carboxylates ( $\nu_{\text{as}} \approx 1560\text{--}1630\text{ cm}^{-1}$ )<sup>[29]</sup> or bending vibrations of water molecules dissolved in the glass ( $\delta \approx 1630\text{ cm}^{-1}$ )<sup>[30]</sup>. The latter assignment, however, is less likely as bending vibrations of water molecules have low absorption coefficients and small half widths.<sup>[31,32]</sup> Asymmetric vibrations of carbonates split into doublets,<sup>[29]</sup> the shoulder could also represent the high-energy component of such a doublet. Due to the large split width, the low-energy doublet component could be hidden by the strong glass band at  $1400\text{ cm}^{-1}$ . The split width,  $\Delta\nu_{\text{as}}$ , is  $\approx 100\text{ cm}^{-1}$  for monodentate carbonates and  $> 300\text{ cm}^{-1}$  for bidentates.<sup>[29]</sup> For carbonates dissolved in glasses,  $\Delta\nu_{\text{as}}$  depends on network connectivity.  $\Delta\nu_{\text{as}} = 77\text{--}105\text{ cm}^{-1}$  and  $\Delta\nu_{\text{as}}$  up to  $295\text{ cm}^{-1}$  were respectively reported for depolymerized and polymerized glasses.<sup>[33]</sup> In soda lime silica glasses such a doublet was found at  $1425$  and  $1485\text{ cm}^{-1}$ .<sup>[31]</sup>

Most strikingly, however, the shoulder at  $1540\text{--}1630\text{ cm}^{-1}$  disappears during heating. This finding shows that related species escape during heating to  $620\text{ }^\circ\text{C}$  and do not cause foaming. However, it cannot be ruled out that other weak absorption bands

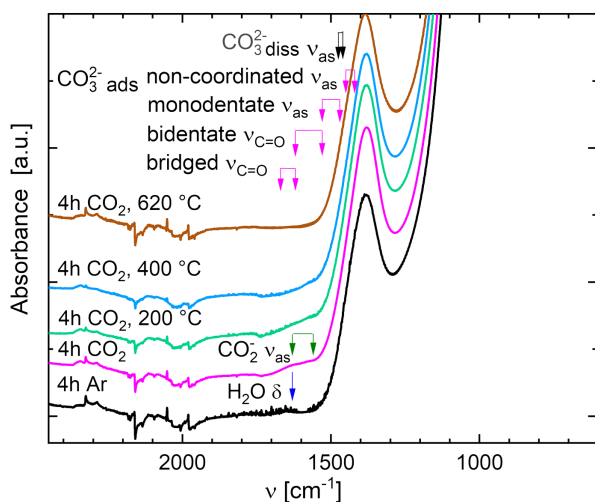


**Figure 5.** ATR–FTIR absorption spectra of K01 glass powders milled as labeled and heated at  $5\text{ K min}^{-1}$  to the temperatures indicated. Curves are normalized to equal height at  $1000\text{ cm}^{-1}$  and separated by an offset value. Arrows indicate the spectral range of stretching ( $\nu$ ) and bending ( $\delta$ ) vibrations of dissolved carbonates ( $\text{CO}_3^{2-}\text{diss}$ ),<sup>[33]</sup> adsorbed carbonates ( $\text{CO}_3^{2-}\text{ads}$ ), carboxylates ( $\text{CO}_2^-$ ), and water molecules ( $\text{H}_2\text{O}$ ).<sup>[30]</sup> For asymmetric stretching vibrations ( $\nu_{\text{as}}$ ), which split into doublets, arrows show the range of the doublet center position.

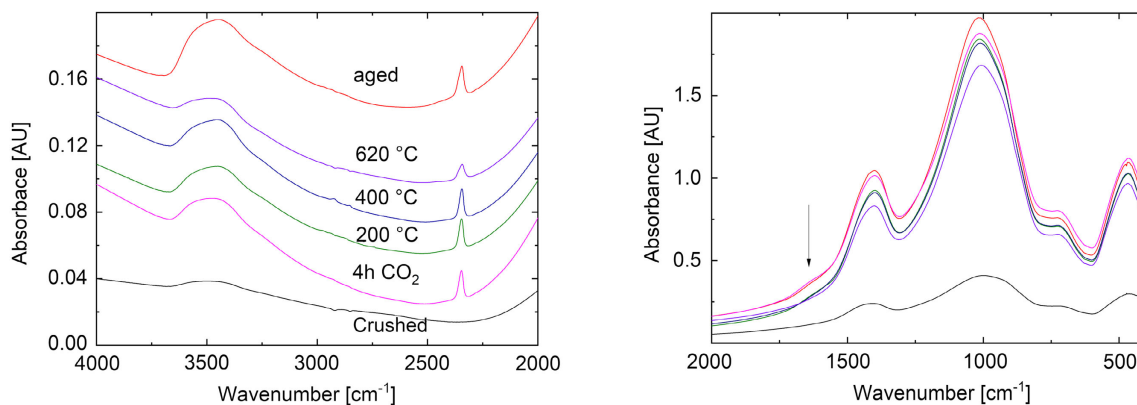
of carbonaceous species are hidden by the strong band at  $1400\text{ cm}^{-1}$ . Furthermore, only species very close to the surface are detectable by ATR–FTIR.

Figure 6 shows FTIR absorption spectra of KBr-pressed pellets containing annealed and re-ground compacts of glass powders 4 h milled in  $\text{CO}_2$ . The band at  $\approx 1000\text{ cm}^{-1}$  is attributed to asymmetric Si–O stretching<sup>[34,35]</sup> as  $\text{SiO}_2$  is the main constituent of our glass. The band at  $\approx 1400\text{ cm}^{-1}$  is most likely caused by  $\text{B}^{\text{III}}$  units.<sup>[36]</sup> The out-of-plane bending of  $\text{B}^{\text{III}}$  groups occurs at  $\approx 750\text{ cm}^{-1}$ .<sup>[37]</sup> The weak band at  $1540\text{--}1630\text{ cm}^{-1}$  in the ATR–FTIR spectra (Figure 5) is also visible in the absorption spectra (arrow) and its intensity decreases upon heating. Figure 6 thus confirms that carbonate groups are most likely located at the surface and are destroyed during heating to  $T_g$ .

The broad peak at around  $3400\text{ cm}^{-1}$  ( $2.9\text{ }\mu\text{m}$ ) in the left figure is caused by OH stretching vibration modes. This band is not only caused by hydrous species in the glass but also contains contributions from the KBr matrix and the KBr/glass powder interface. These contributions vary from sample to sample and cannot be completely eliminated by subtraction of a spectrum of a glass-free KBr-pressed pellet. Nevertheless, some systematic trends are visible for the OH stretching vibration band. While the spectrum of the crushed sample is probably dominated by the KBr-related contributions, the higher absorbance of the  $\text{CO}_2$ -milled samples is attributed to hydrous species within the glass bulk and on the surface. The peak intensity slightly decreases after heating at  $5\text{ K min}^{-1}$  to  $620\text{ }^\circ\text{C}$  but does not change for the samples heated to  $200$  and  $400\text{ }^\circ\text{C}$ . This finding correlates with what one might expect for diffusive degassing of dissolved water. Aging for 11 months in air significantly increases the intensity of the peak at  $3400\text{ cm}^{-1}$ , indicating progressive water adsorption or corrosion phenomena.

Most interesting in Figure 6, left, however, are small single peaks at  $2344\text{ cm}^{-1}$  in the  $\text{CO}_2$ -milled samples with a full width at half height (FWHH) of  $\approx 23\text{ cm}^{-1}$  for the starting powder and the sample heated to  $400\text{ }^\circ\text{C}$ . After heating to  $620\text{ }^\circ\text{C}$ , the FWHH slightly increases to  $27\text{ cm}^{-1}$ . The wavenumber is typical for the asymmetric stretching vibration of  $\text{CO}_2$  molecules. However, free  $\text{CO}_2$  gas molecules are characterized by a doublet with a large FWHH of  $\approx 60\text{ cm}^{-1}$  due to rotation-vibration coupling. The observed peak at  $2344\text{ cm}^{-1}$  is therefore due to  $\text{CO}_2$  molecules unable to rotate. Such peaks were attributed to dissolved  $\text{CO}_2$  molecules in numerous silicate and aluminosilicate glasses<sup>[33,38]</sup> of relatively open network structures.<sup>[39]</sup> The single peak with small half-width at  $2344\text{ cm}^{-1}$  thus indicates that the detected  $\text{CO}_2$  is not encapsulated as a free gas in micropores but as tightly entrapped as an dissolved molecule. Quite similar to the peak at  $3500\text{ cm}^{-1}$  indicating dissolved water, this  $\text{CO}_2$  peak remains constant during heating to  $400\text{ }^\circ\text{C}$  and slightly decreases after heating to  $620\text{ }^\circ\text{C}$ . This behavior indicates a similar diffusion-limited degassing mechanism.

The amount of molecular  $\text{CO}_2$  can be estimated from the height of the  $2344\text{ cm}^{-1}$  peak. The linear molar absorption coefficient for the peak ( $\epsilon_{2344}$ ) varies only slightly with glass composition. Based on eight compositions reported in Figure 3 in the study by Behrens et al.,<sup>[38]</sup> the average of  $\epsilon_{2344}$  is  $940 \pm 160\text{ L}\cdot\text{mol}^{-1}\cdot\text{cm}^{-1}$ . The thickness of the KBr-pressed



**Figure 6.** FTIR absorption spectra of KBr-pressed pellets for K01 glass powders jaw-crushed, 4 h milled in CO<sub>2</sub> and heated at 5 K min<sup>-1</sup> to the indicated temperature. The aged sample was stored for 11 month in ambient air. Curves in the left graph have been shifted by an offset for clarity. The arrow marks the weak shoulder which may be caused by carbonate vibration. Colors on right side correspond to those assigned on the left side and in Figure 5.

pellets was  $1.1 \pm 0.1$  mm, containing 2.5 wt% glass with a density of  $3613 \text{ g L}^{-1}$ .<sup>[24]</sup> Using a modified Lambert–Beer law,<sup>[38]</sup> it was concluded that the samples milled for 4 h in CO<sub>2</sub> contain  $209 \pm 12$  ppm ( $1\sigma$ ) molecular CO<sub>2</sub>, which is not changed by heating up to 400 °C. Heating up to 620 °C reduces this amount by half. The error in this estimate is probably much higher than the  $1\sigma$  value given above, as it is affected by the preparation of KBr-pressed pellet, that is, size and distribution of glass particles in the pellet.

## 2.6. XPS

**Table 2** shows elements detected by XPS at the outermost surface ( $\approx 10$  nm) of glass powders crushed, 4 h milled in Ar, 4 h milled in CO<sub>2</sub>, as well as a powder 4 h milled in CO<sub>2</sub>, heated at 5 K min<sup>-1</sup> to 620 °C and quenched in air. In addition to the main glass components, a noticeable amount of carbonaceous species is evident. The nature of these species can be inferred from the XPS spectra in **Figure 7**. Gaussians fitting indicates the presence of four different peaks. Peak I (285 eV), most prominent in all cases, is attributed to C–H environmental contaminations (adventitious carbon).<sup>[40]</sup> Peak II (281 eV) is due to the carbon tape used to fix the sample and peak III (277 eV) is due to the sample holder.

**Table 2.** XPS atomic concentration in percentage. The effect of the sticking tape was corrected. O 1s = 532 eV (Me<sub>x</sub>O<sub>y</sub>, organic O), Ba 3d<sub>5/2</sub> = 780 eV (Ba<sup>2+</sup>), and Zn 2p<sub>3/2</sub> = 1022 eV (Zn<sup>2+</sup>). C 1s = cumulating 285 eV (C–H contaminations), 277 eV (sample holder), and 289 eV (carbonates or oxalates).

	O 1s	Si 2s	Ba 3d <sub>5/2</sub>	Zn 2p <sub>3/2</sub>	C 1s	C 1s <sup>a)</sup>
Crushed	48.0	11.2	7.1	4.0	27.6	0
4 h Ar	48.1	13.6	10.7	4.0	22.9	1.19
4 h CO <sub>2</sub>	53.3	9.4	9.4	3.5	22.6	3.06
4 h CO <sub>2</sub> , T = 620 °C	53.2	11.2	8.7	3.0	22.1	0

<sup>a)</sup>C 1s refers to peak IV. Traces of Mn between 0.7 and 2.1% are not shown.

Only peak IV noticeably varies with powder preparation and its binding energy (290 eV) matches that of carbonates<sup>[41]</sup> or oxalates.<sup>[42]</sup> Peak IV is most intensive for the glass powder 4 h milled in CO<sub>2</sub>. It also appears for the powder milled in Ar, where its peak intensity and the associated carbon content (Table 2, C 1s\*) are lower. As carbon is basically absent during milling, this analysis proves that glass surfaces generated by milling in Ar were later contaminated with carbonaceous species. No such species, however, were detected for the crushed sample and the powder 4 h milled in CO<sub>2</sub> and heated to 620 °C. Consistent with the IR observations, these findings indicate that carbonaceous species escape from the surface during heating.

## 2.7. TOF-SIMS

### 2.7.1. Surface Analysis

Ionized molecular and atom fragments analyzed by TOF-SIMS on the surface of differently prepared glass powders are shown in **Table 3**. Columns II and III show that milling in CO<sub>2</sub> instead of Ar increases the concentration of Ba and C species at the sample surface. This increase is most obvious for Ba, BaCO<sub>3</sub>, and carboxylate (BaCO<sub>2</sub>). Vice versa, heating to 620 °C (Columns IV and V) caused a strong decrease in Ba and C species. Consistent with the other data, the TOF-SIMS analyses indicates that carbonaceous species trapped during powder processing escape from the outermost surface during heating to 620 °C.

### 2.7.2. Depth Profiles

Due to the large analyzed surface area of  $100 \times 100 \mu\text{m}$ , TOF-SIMS depth profiling experiments require samples larger than that size. To mimic surface contamination of carbonaceous species during milling, glass particles of  $\approx 3$  mm in size were milled together with the same mass of jaw-crushed powder for 1 h in CO<sub>2</sub>. **Figure 8** shows a laser scanning (a) and a SEM (b) micrograph of the surface of such a glass particle. The upper-right part of Figure 8a shows a freshly fractured surface. Bright areas below this fracture indicate unresolved small adhering glass

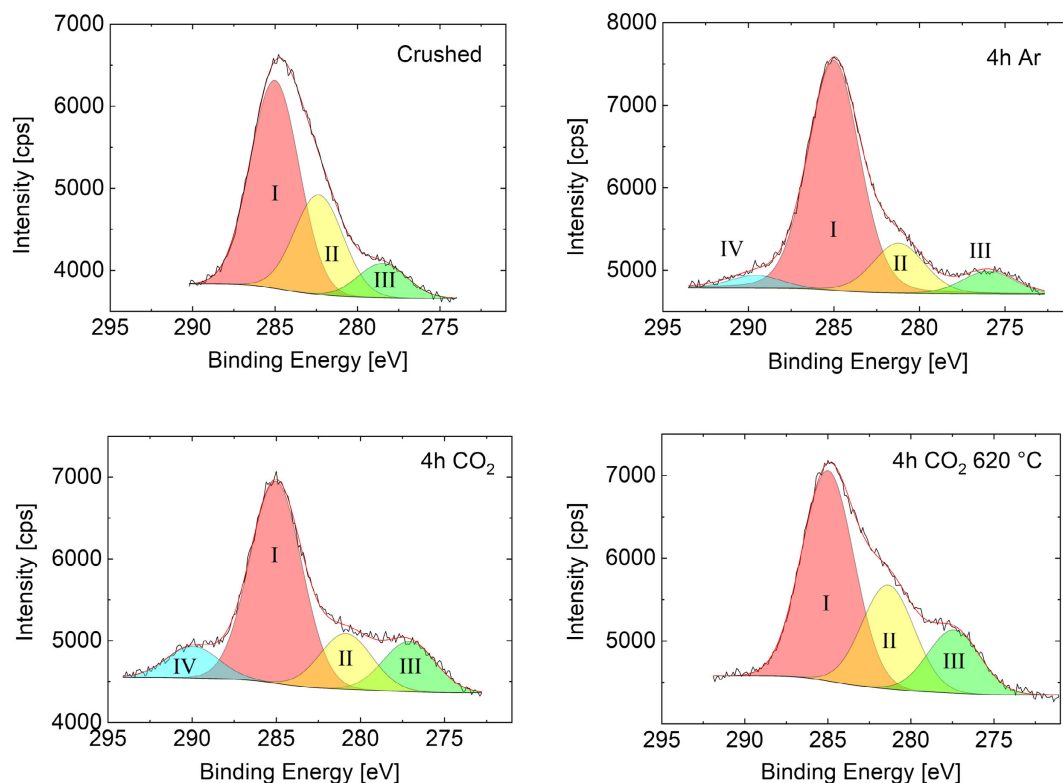


Figure 7. C1s XPS spectra of differently prepared K01 glass powders.

**Table 3.** TOF–SIMS mean counts versus mass peak areas normalized to Si for 4 h-milled glass powders. Column I presents mass numbers of detected species. Columns II and III compares their relative abundance for the powders 4 h milled in Ar and CO<sub>2</sub>. Columns IV and V show results of a later experiment (3 months) comparing the powder 4 h milled in CO<sub>2</sub> before and after heating to 620 °C, respectively. Δ<sub>1</sub> and Δ<sub>2</sub> are the relative differences between the two left neighbored columns.

	I: Mass [u]	II: 4 h Ar	III: 4 h CO <sub>2</sub>	Δ <sub>1</sub> (%)	IV: 4 h CO <sub>2</sub>	V: 4 h CO <sub>2</sub> 620 °C	Δ <sub>2</sub> (%)
CO <sub>2</sub>	43.9842	0.0582	0.0823	+41	0.1017	0.0439	-57
Ba	137.9155	0.0276	0.0408	+47	0.0564	0.0316	-44
BaO	153.875	0.0246	0.0294	+19	0.0323	0.0115	-64
BaCO <sub>2</sub>	181.8756	0.0039	0.0056	+43	0.0085	0.0044	-48
BaCO <sub>3</sub>	197.8615	0.0183	0.0267	+47	0.0338	0.0120	-65
BaC <sub>2</sub> O <sub>4</sub>	225.8948	0.0014	0.0019	+35	0.0032	0.0013	-58

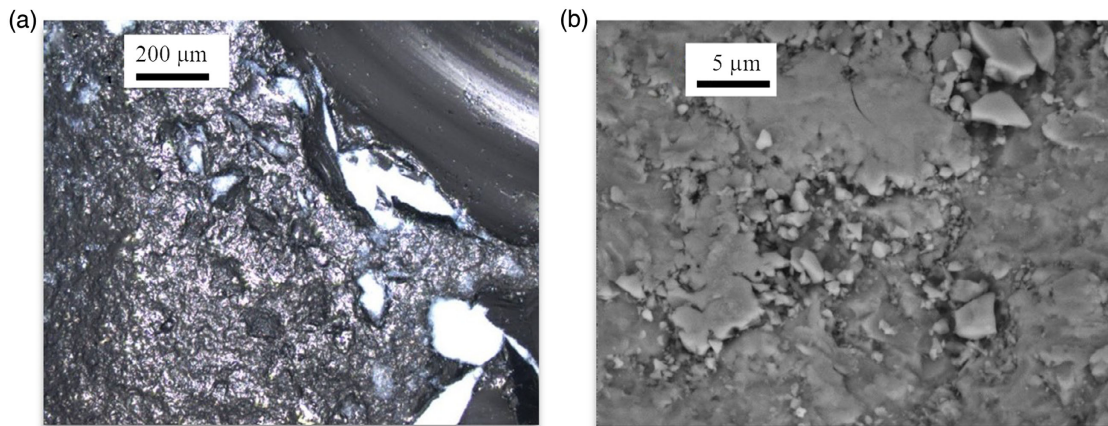
particles agglomerated in surface depressions (“screes”). Detailed SEM studies (not shown) did not reveal plastic flow or sintering within these regions. The lower left part of Figure 8a represents the dominating surface for the given milling condition. A more detailed SEM micrograph of this damaged surface (Figure 8b) hints plastic deformation and reagglomeration during milling.

Figure 9 compares TOF–SIMS depth profiles measured on a freshly fractured glass surface (left), a 3 mm glass particle exposed to 1 h CO<sub>2</sub> milling (center), and a glass particle likewise

milled after heating to 620 °C prior to the measurement (right). The spectra for glass particles exposed to 1 h milling in CO<sub>2</sub> were taken from surface sections resembling the lower left part of Figure 8a. A bulk glass sample freshly fractured in air prior to the measurement is shown for comparison. Intensities of fragments are normalized with the best detectable species BO<sub>2</sub><sup>-</sup> measured at 500 nm depth. CO<sub>3</sub><sup>-</sup> was not measurable because its mass number ( $m/e \approx 60.009$ ) interferes with SiO<sub>2</sub><sup>-</sup> ( $m/e \approx 60.084$ ).

The most abundant fragments, BO<sub>2</sub><sup>-</sup>, BO<sup>-</sup>, SiO<sub>2</sub><sup>-</sup>, Si<sup>-</sup>, and O<sub>2</sub>, represent major components of the glass K01. Minor amounts of CO<sub>2</sub><sup>-</sup>, CO<sub>2</sub>Ba<sup>-</sup>, and CO<sub>3</sub>Ba<sup>-</sup> fragments were also detected. However, their abundance does not correlate with the applied surface preparation (crushed, milled as well as milled and subsequently heated) and their depth profiles do not indicate any surface near enrichment.

Most strikingly, pronounced surface enrichment of carbon (C<sup>-</sup>) is evident in Figure 9 accompanied by sulfur species (S<sup>-</sup> and SO<sub>2</sub><sup>-</sup>). This effect most likely results from C–H environmental contaminations<sup>[40]</sup> as all samples were exposed to air during storage and handling. Such contamination was already detected by XPS and may explain the large total carbon detected by total carbon analysis (Table 1). Due to the large analyzed area (100 × 100 μm<sup>2</sup>), the depth profiles in Figure 9 are strongly affected by surface roughness, cracks, and adhering particles. Thus, the profile recorded is in part an artifact of the measurement. The even more pronounced C<sup>-</sup> profile seen for the sample heated to 620 °C does not necessarily result from heating. It more



**Figure 8.** a) Laser scanning and b) SEM micrographs of the surface of a 3 mm glass particle exposed to 1 h milling in CO<sub>2</sub>. Figure 8b shows a detail of the lower-left part of Figure 8a.

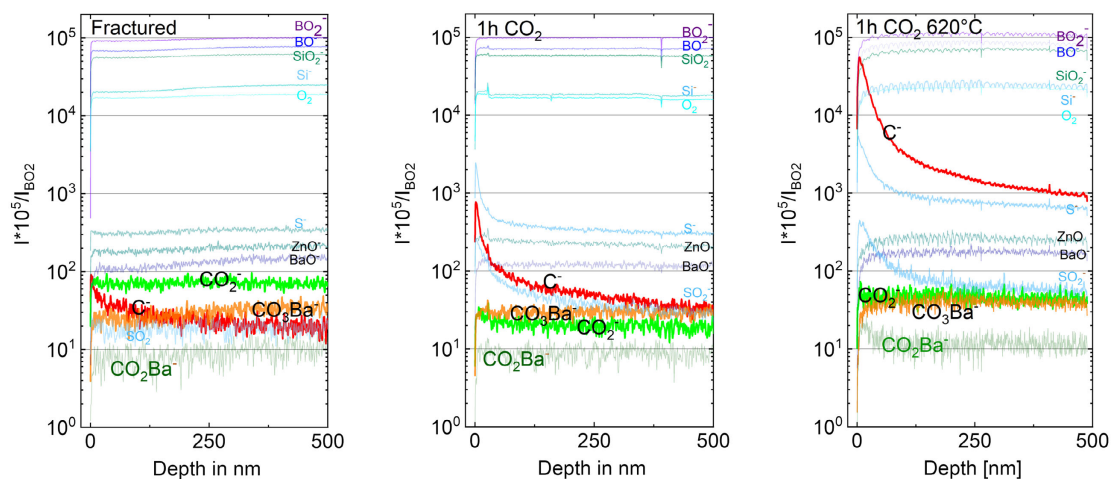


**Figure 9.** TOF-SIMS depth profiles. Fractured: 1 mm glass frit particle freshly fractured prior to the measurement; 1 h CO<sub>2</sub>: 3 mm glass particle exposed to 1 h milling in CO<sub>2</sub>; 1 h CO<sub>2</sub> at 620 °C: similar glass particle exposed to 1 h milling in CO<sub>2</sub> and heated to 620 °C.

likely reflects different degrees of mechanical damage in different surface sections. This assumption is supported by analogous TOF-SIMS experiments on K01 glass particles exposed to 15 min milling in CO<sub>2</sub>, where similar C<sup>-</sup> profiles were found before and after heating.

### 3. Discussion

Agea-Blanco et al.<sup>[24]</sup> have demonstrated that foaming of sintered powder compacts of the barium silicate glass K01 strongly depends on milling duration and atmosphere. Foaming intensity increased in the order Ar ≈ N<sub>2</sub> < air < CO<sub>2</sub> and VHE degassing studies showed that foaming is mainly driven by C, CO, and CO<sub>2</sub>, even for powders milled in Ar or N<sub>2</sub>. It was therefore concluded that foaming is mainly caused by carbonaceous species adsorbed at the glass powder surface during milling and powder storage.

The present study is focused on the nature of these species and the mechanisms of species trapping. To intensify foaming, K01

glass powders were milled in CO<sub>2</sub> for several hours. Figure 1 shows that this milling caused substantial foaming, in particular for the powder 4 h milled in CO<sub>2</sub> (*s<sub>A</sub>* ≈ 380%), whereas much less-intensive foaming was reported in the study by Agea-Blanco et al.<sup>[24]</sup> for shorter milling in air (*s<sub>A</sub>* ≈ 30% for 30 min milling). Table 1 concordantly shows that large amounts of total carbon were found for the powder 4 h milled in CO<sub>2</sub> (1428 wt.ppm).

#### 3.1. Mechanisms of Species Trapping

As the most intuitive and simple foaming mechanism, stable surface carbonates, formed during milling at the glass surface, could be assumed not to escape during heating and encapsulated during sintering.

Although consistent with the similar temperature range of BaCO<sub>3</sub> decomposition and foaming (Figure 1, 4), this simple mechanism, however, cannot explain why no surface enrichment of BaCO<sub>3</sub> could be detected for powders heated to temperatures

above 600 °C by XPS (Figure 7) and TOF-SIMS (Figure 9). Further, assuming that gas uptake entirely proceeds during milling does not explain why foaming is mainly driven by carbon-related gases even for milling in Ar atmosphere (Figure 3A), where CO<sub>2</sub> is not present. In a similar sense, surface species stability as the only trapping mechanism would not explain why Ar does not fully escape from the glass powder compact during heating in air as it is clearly proved by its contribution to foaming. Also, the enhanced Ar degassing above  $T_g \approx 650 - 780$  °C in Figure 3 is unlikely to be caused by Ar desorption. Finally, it would be difficult to understand why CO<sub>2</sub> trapped during milling does not escape during heating to 620 °C (Figure 6).

These findings indicate that species trapping could be more complex. On the one hand, initially adsorbed gases might be replaced by or react to more stable species. On the other hand, milling and powder compaction may cause microporosity, surface cracks, or even micro plastic flow phenomena. These effects may provide glass surface areas, which are quite differently accessible for gas exchange. This way, species uptake, evolution, and encapsulation may be locally delayed or enhanced and may extend over different powder processing steps. **Figure 10** schematically shows the mechanism from the initial adsorption to foaming for intensively milled glass powders.

### 3.1.1. Initial Gas Uptake

Glass surfaces freshly fractured during milling will be instantaneously covered with gas molecules of the milling atmosphere.

As this process depends on powder surface area and adsorption kinetics (physisorption vs. chemisorption), foaming intensity strongly depends on milling duration<sup>[24]</sup> and atmosphere (Figure 1, see the study by Agea-Blanco et al.<sup>[24]</sup>). In particular, prolonged milling will cause surface cracks and particle agglomerates, as illustrated by the boxes of Figure 10 and supported by Figure 8. This effect substantially increases the specific powder surface area available for gas uptake. Due to the difficult gas transport into cracks and particle aggregates, however, initial gas uptake may be delayed and can go on after milling during storage or sample handling. For milling in Ar, and storage in air, for example, different gas species can consecutively contribute to the initial gas uptake. This effect easily explains the increase in foaming intensity after prolonged storage in air.<sup>[24]</sup>

### 3.1.2. Species Evolution

Sorption/desorption is a dynamic equilibrium reaction and more reactive gases such as H<sub>2</sub>O and CO<sub>2</sub> are more strongly bound by chemisorption than gases such as N<sub>2</sub> or Ar. Even in Ar atmosphere, surface sites are thus progressively occupied by H<sub>2</sub>O and CO<sub>2</sub> even if only traces are present. This process involves the formation of carbonaceous species (indicated by green color in Figure 10), which finally leads to their dominance as the major source of foaming (see the study by Agea-Blanco et al.<sup>[24]</sup> Figure 3), as supported by XPS and TOF-SIMS. Sorption/desorption phenomena also explain the large total carbon content of the powder milled in Ar, that is, why Ar, adsorbed during

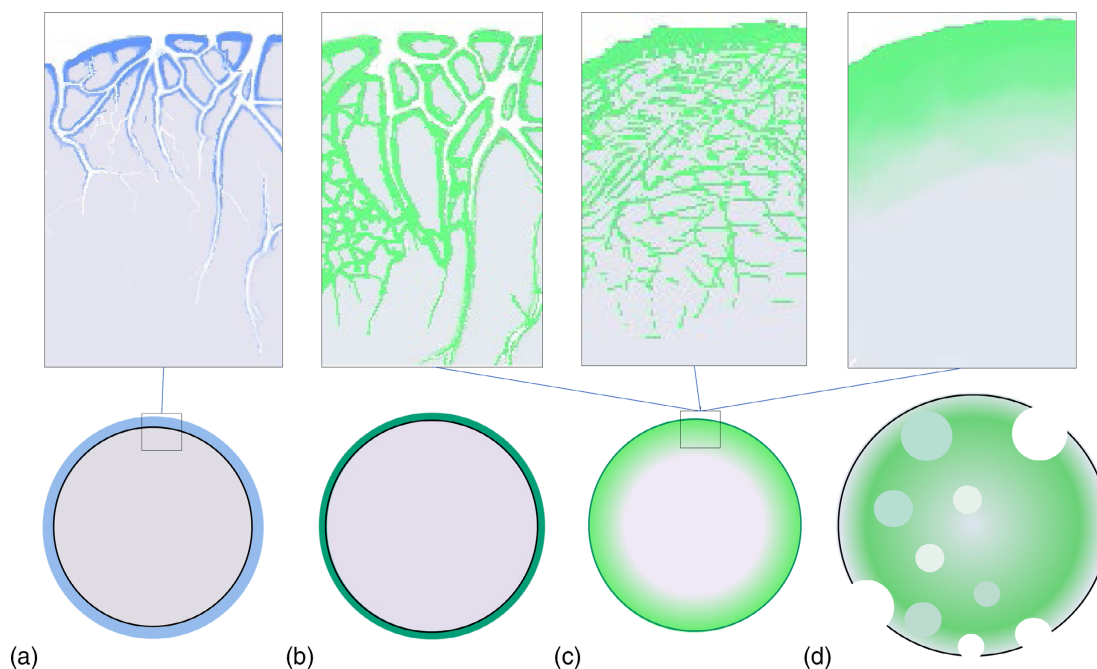


**Figure 10.** Schematic illustration of different mechanisms responsible for foaming. Mechanism (a) indicates the initial gas uptake during milling or later storage. Mechanism (b) indicates that initially adsorbed species can be replaced by or can chemically react to other more stable species. This species evolution is indicated by a change of color. Mechanism (c) indicates different mechanisms of trapping the still remaining stable species beneath the surface. Such mechanisms comprise microencapsulation, mechanical dissolution, and inward diffusion. Mechanism (d) indicates diffusive degassing and foaming. Whereas initial gas uptake (a) most likely occurs during milling, species evolution (b) and trapping (c) can simultaneously occur during different powder processing steps.



milling, was replaced by CO<sub>2</sub> (and H<sub>2</sub>O) during later sample handling and storage in air. Sorption/desorption equilibria are also indicated by DTA measurements, proving that the vast majority of carbonaceous species desorbs prior to sintering.<sup>[24]</sup>

As part of foaming species evolution, the interaction of H<sub>2</sub>O and CO<sub>2</sub> with the glass surface may also cause early glass corrosion. Consistently, TOF–SIMS data show more enrichment of Ba on glass surfaces milled in CO<sub>2</sub> than for milling in Ar. Thus, by diffusion of Ba from beneath the surface, precursors of BaCO<sub>3</sub> can be formed. This effect continues with milling duration as this reaction steadily goes on and as the surface area further increases. Corrosion may additionally benefit from local heat generation during milling. However, corrosion products often have low thermal stability and are largely destroyed during heating to the sintering temperature. As the TOF–SIMS measurements on the heated samples show, Ba is depleted again at the surface, that is, the corrosion process is partially reversed, at least during its initial phase.

As the evolution of foaming species depends on time, temperature, species stability, and concentration, it will proceed through all processing steps. It can be complicated by tribochemical effects, local heating during milling, and the formation of dangling bonds during fracturing,<sup>[43]</sup> which may even provide local oxygen deficiency inside microcracks and cavities, favoring carbonaceous species to decompose to carbon during heating. The reducing effect of soda lime silica surfaces fractured in vacuum was demonstrated by Baptist and Levy.<sup>[44]</sup> Last not least, the species decomposition, which finally causes bubble growth and foaming, may be considered as part of foaming species evolution.

### 3.1.3. Foaming Species Trapping

*Microencapsulation:* Foaming species must remain trapped during heating to the temperature of foaming to be able to cause foaming. Encapsulation of stable surface species, for example, BaCO<sub>3</sub>, into closed pores during sintering, is the most simple and intuitive trapping mechanism. Carbonate decomposition can thus increase the CO<sub>2</sub> gas pressure inside closed pores, thus driving bubble growth and foaming.

However, as degassing depends on time, temperature, species stability, and concentration, it can be substantially delayed within cracks or micropores. With increasing milling duration, the fraction of submicrometer particles strongly increases. Due to adhesion forces, these particles strongly tend to agglomerate and can form difficult accessible micropores. Local forces and heating during milling can promote this effect. Moreover, uniaxial powder compaction can narrow interconnecting cavities, in particular, in the outer shell of powder compacts. This effect further impedes the outward diffusion of gas components and favors the formation of a stagnant atmosphere at ambient pressure. This effect scales with the size of powder compacts.

Due to bottlenecks in the pore space, the pathways for gas molecules to the surrounding atmosphere are artificially prolonged and even less stable species as Ar may be retained in agglomerates till the temperature range of sintering is reached. In addition, as sintering strongly depends on particle size, submicro particles can start sintering up to 100 K below the sintering onset temperature of microparticles.<sup>[1]</sup> Moreover, the surface near

dissolved water can locally decrease viscosity, which would further promote this effect. This scenario is consistent with Figure 2 and would easily explain the intensive Ar degassings spikes > 840 °C in Figure 3.

*Mechanical Dissolution:* The presence of CO<sub>2</sub> molecules unable to rotate after 4 h milling in CO<sub>2</sub> (Figure 6) cannot be explained, assuming encapsulation of gaseous CO<sub>2</sub>. Intensive milling, however, can provide other trapping mechanisms. The experiments with large embedded glass pieces have demonstrated that punctual forces and local heating can initiate plastic deformation during milling (Figure 8b). Former surface layers can thus be transferred into the interior of the glass, which is referred to as “mechanical dissolution” or “burying” below. Sorption of gas molecules can also occur inside glass grains when microcracks are temporarily opened. Similarly, Kalinkina et al.<sup>[45]</sup> explained substantial CO<sub>2</sub> uptake during intensive milling of Ca and Mg silicate minerals by the formation and migration of dislocations<sup>[46]</sup> and the propagation of micro- and submicro cracks. Penetration of CO<sub>2</sub> into mineral grains and the formation of CO<sub>3</sub><sup>2-</sup> were discussed to occur not only along cracks but also directly into the bulk.<sup>[43]</sup>

Mechanical dissolution or burying would easily explain why CO<sub>2</sub> molecules unable to rotate can be trapped even during milling although substantial diffusion seems highly unlikely to occur below T<sub>g</sub>. This mechanism may also encapsulate Ar, water, and carbonaceous species.

*Inward Diffusion:* Above T<sub>g</sub>, inward diffusion may occur as a further trapping mechanism. This mechanism can be considered as an initial degassing step for gaseous or surface species trapped in closed micropores. Depending on the thermal species stability and concentration, inward diffusion may even proceed during sintering and foaming.

Below T<sub>g</sub>, however, inward diffusion does not essentially contribute to species trapping. Diffusion of Ar and CO<sub>2</sub> occurs through interstices in the glass structure and is similarly fast.<sup>[39]</sup> The diffusion of carbonate is considerably slower and determined by the dynamics of the network.<sup>[47]</sup> Even in the open fused silica structure, the (extrapolated) diffusion coefficient of CO<sub>2</sub> at 600 °C is only 2.5 · 10<sup>-18</sup> m<sup>2</sup>s<sup>-1</sup>, corresponding to a diffusion length of 0.13 μm after 1 h. Thus, for the more densely packed barium disilicate glass, no significant diffusion of Ar or carbonaceous species is expected during heating of the glass below T<sub>g</sub>. Similarly, diffusion by short-term heating and melt formation during milling will not lead to deeper intrusion of the species into the glass grains. The thermal diffusivity of glasses in the order of 1 · 10<sup>-6</sup> m<sup>2</sup>s<sup>-1</sup><sup>[48]</sup> is several orders of magnitude higher than any measured Ar diffusion coefficient in silicate melts (D<sub>Ar</sub> ≈ 1 · 10<sup>-10</sup> m<sup>2</sup>s<sup>-1</sup><sup>[49]</sup>). Hence, heat dispersion occurs much faster than diffusion of gas components in the melt. In conclusion, below T<sub>g</sub> diffusion can only locally redistribute carbonaceous species in glasses, but it does not enable long-range transport into the interior of glass grains.

### 3.1.4. Diffusive Degassing and Foaming

Further heating will cause diffusive degassing, in particular, under vacuum, during VHE. Outward diffusion can easily explain the smooth increase in degassing activity of Ar, carbon-

related species, and SO<sub>2</sub> above  $T_g$  in Figure 3. The diffusive nature of this effect is indicated by previous studies on water degassing of soda lime silica glasses<sup>[25]</sup> and by the similar degassing behavior of Ar for the glass powder milled in Ar as Ar unlikely desorbs at such high temperatures. The similar degassing behavior of Ar and CO<sub>2</sub> above  $T_g$  (Figure 3) is consistent with their similar diffusivity in fused silica and in aluminosilicate glasses.<sup>[39,50]</sup> Likewise, the diffusive nature of this degassing mechanism is indicated by the similar degassing of SO<sub>2</sub>, presumably used as a fining agent for the commercial glass K01 under study. Further, outward diffusion of all these species is supported by the sinter-induced drop of their degassing activity > 740 °C (Figure 3 left). As all species contribute to gas bubble bursting, this drop does not reflect degassing exhaustion.

In the interior of densified powder compacts or particle aggregates, the interplay of viscous flow and volatile diffusion later controls bubble expansion and bursting. At the onset of foaming, bubbles are most frequent at the edges of large grains and in regions with fine-grained material but absent in the interior of large grains (Figure 2). This observation supports the fact that burial of carbonaceous species occurs primarily at edges and rims, and diffusive redistribution was possible only locally.

### 3.1.5. Foaming Species Contributions

*Species Dissolved during Glass Melting:* As discussed earlier, different species differently trapped during milling and powder processing could contribute to foaming. Volatiles dissolved during glass melting, as fining agents like SO<sub>2</sub> (Figure 3) or from raw materials and gas atmosphere (H<sub>2</sub>O, CO<sub>2</sub>), however, do not essentially contribute to sinter foaming because of their low solubility in the high-temperature melts. This was confirmed by comparing VHE degassing curves of fine and coarse K01 glass powders in the study by Agea-Blanco et al.<sup>[24]</sup> Likewise, the strong effect of milling duration on foaming<sup>[24]</sup> proves that the vast majority of foaming species is trapped at the powder surface.

*Milling Atmosphere:* Gases encapsulated during milling or powder compaction do not essentially contribute to foaming. This conclusion is supported by Figure 3, showing that Ar encapsulated during 4 h milling in Ar atmosphere only partially contributes to foaming even though essential microporosity can be expected. The only minor contribution of encapsulated milling atmosphere was already demonstrated in the study by Agea-Blanco et al.,<sup>[24]</sup> estimating the possible foaming contributions of milling gases encapsulated during sintering at 0.8 relative density. Another supporting observation is the strong effect of milling duration on foaming intensity reported in the study by Agea-Blanco et al.<sup>[24]</sup>

*Absorbed Water:* Surface-adsorbed water might be reasonably expected as a source of foaming. It is well known that H<sub>2</sub>O is strongly adsorbed on glass surfaces and promotes glass corrosion by reaction with the silicate network. However, Figure 3 and the VHE degassing studies in the study by Agea-Blanco et al.<sup>[24]</sup> clearly prove that H<sub>2</sub>O almost fully desorbs during heating and does not essentially contribute to foaming (spikes in Figure 3).

*Mechanically Dissolved CO<sub>2</sub>:* FTIR absorption spectra in Figure 6 and the earlier discussion indicate that CO<sub>2</sub> molecules are mechanically dissolved beneath the glass surface during

milling. Using the estimated content of CO<sub>2</sub> molecules present after heating to 600 °C ( $\approx 100 \mu\text{g/g}$ , see Section 2.5), we calculated the corresponding volume increase of the powder compact, assuming that these molecules are completely transferred into bubbles. For 1 bar inner pressure of the bubbles,  $s_A \approx 73\%$  is expected at 800 °C. This value is much lower than  $s_A > 380\%$ , as observed for the powder milled for 4 h in CO<sub>2</sub> in Figure 1, which indicates that mechanically dissolved CO<sub>2</sub> is not the dominating source of foaming.

*Adventitious Carbon:* As another possible source of CO<sub>2</sub> degassing, TOF-SIMS and XPS revealed C-H environmental contaminations. Such species may have been encapsulated or mechanically dissolved during milling and powder compaction and can thus survive during heating. However, C-H species can only contribute to foaming, if oxygen is available in the glass interior, that is, only if CO<sub>2</sub> can be formed in closed gas bubbles or inside the glass. Essential CO<sub>2</sub> formation is therefore limited by oxygen diffusion from the ambient atmosphere. Diffusion data for O<sub>2</sub> in silicate glasses and melts under essentially dry conditions are very rare<sup>[49]</sup> and do not exist for the glass under study.

Instead, oxygen diffusivity can be roughly estimated using the Eyring equation,  $D_{O_2} = kT/(\lambda\eta)$ , where  $k$ ,  $\lambda$ ,  $\eta$ , and  $T$ , respectively, denote the Boltzmann constant, jump distance, viscosity, and absolute temperature.<sup>[47]</sup> At 800 °C, the K01 melt under study has a viscosity of  $3.1 \cdot 10^5 \text{ Pa}\cdot\text{s}$ .<sup>[24]</sup> Assuming  $\lambda = 5 \cdot 10^{-10} \text{ m}$ ,  $D_{O_2} \approx 9.3 \cdot 10^{-18} \text{ m}^2\text{s}^{-1}$  is estimated, corresponding to a diffusion length  $(2Dt)^{0.5}$  of  $\approx 820 \text{ nm}$  after 1 h. As diffusion lengths in the millimeter range are required after sintering (>750 °C, Figure 1), it is quite obvious that the transport of oxygen is far too low to produce significant CO<sub>2</sub> during foaming. Oxygen transport can be faster when H<sub>2</sub>O is the diffusing species,<sup>[39,47]</sup> but the generated hydrogen (e.g.,  $2 \text{ H}_2\text{O} + \text{C} = \text{CO}_2 + 2 \text{ H}_2$ ) will counteract the oxidation reaction. Thus, C-H contaminations are very unlikely to provide major foaming species for the K01 glass compacts and heating conditions of our study.

*Carbonates:* Stable carbonates formed during milling, later storage, or heating could be assumed not to escape during heating and encapsulated during sintering before being decomposed and causing foaming. This assumption is consistent with Figure 1 and 4, indicating both BaCO<sub>3</sub> decomposition and foaming between 700 and 900 °C. Further, evidence for the formation of carbonate-like species during milling is given by XPS spectroscopy and supported by IR spectroscopy.

However, XPS (Figure 7), IR spectroscopy (Figure 5), and TOF-SIMS (Table 3) indicate that carbonates should disappear from the surface during heating well before sintering and foaming temperatures are reached. These findings are consistent with the DTA studies in the study by Agea-Blanco et al.,<sup>[24]</sup> which proves that the vast majority of carbonaceous species escape during heating to the sintering temperature.

In contrast, our experiments do not exclude that carbonates mechanically dissolved beneath the surface or encapsulated in micropores of tight particle aggregates may provide a major foaming source for several reasons. First, the DTA experiment in the study by Agea-Blanco et al.<sup>[24]</sup> proved that the fraction of carbonaceous species remaining after heating to sintering temperature could cause substantial foaming. Similarly, estimations based on the ideal gas equation show that only  $\approx 10\%$  of the

measured total carbon content of the powder milled for 4 h in CO<sub>2</sub> would easily explain the observed foaming intensity. ATR–FTIR and XPS are sensible only within the outermost surface region of the glasses, and carbonates mechanically dissolved or encapsulated in particle aggregates could not be detected. IR transmission spectroscopy does not suffer from this disadvantage but is limited by the intense and broad vibration band of trigonal boron at 1400 cm<sup>-1</sup>. Finally, TOF–SIMS cannot unambiguously detect carbonates in silicate glass due to similar mass numbers of CO<sub>3</sub> and SiO<sub>2</sub>.

#### 4. Conclusion

The pronounced foaming of the intensively milled commercial BaO–Al<sub>2</sub>O<sub>3</sub>–ZnO–B<sub>2</sub>O<sub>3</sub>–SiO<sub>2</sub> glass powders under study is primarily driven by carbonaceous species but not caused by surface carbonates encapsulated during sintering. Thus, ATR–FTIR and FTIR absorption studies solely show weak shoulders between 1550 and 1630 cm<sup>-1</sup>, possibly originating from carbonates, but they progressively disappeared upon heating. This observation is confirmed by XPS and TOF–SIMS measurements comparing milled with milled and annealed glass powders and DTA studies reported in the study by Agea-Blanco et al.,<sup>[24]</sup> proving that the vast majority of carbonaceous species escape during heating to the sintering temperature.

In contrast, our experiments cannot exclude that foaming is driven by carbonaceous species mechanically dissolved beneath the surface or encapsulated within tight particle aggregates. This is because ATR–FTIR and XPS are sensible only in the outermost surface region, IR transmission spectroscopy is limited by the intense absorption of trigonal boron at 1400 cm<sup>-1</sup>, and TOF–SIMS cannot unambiguously detect carbonates in silicate glasses due to similar mass numbers of CO<sub>3</sub> and SiO<sub>2</sub>.

Mechanical dissolution is necessarily required to explain the presence of CO<sub>2</sub> molecules unable to rotate the FTIR absorption spectra of powders milled in CO<sub>2</sub>. Their large amount indicates that this trapping mechanism could essentially contribute to foaming.

Summing up, our favored explanation for the pronounced foaming of the glass powder compacts under study is the decomposition of carbonate-like species trapped via mechanical dissolution or microencapsulation beneath the surface.

#### 5. Experimental Section

**Materials:** This study was conducted on a commercial barium alumino borosilicate glass used for SOFC sealing (K01, KERAFOIL keramische Folien GmbH, Eschenbach, Germany; also supplied by Fraunhofer IKTS, Dresden, Germany<sup>[7]</sup>). The glass transition temperature,  $T_g = 649$  °C, and the coefficient of thermal expansion,  $CTE_{25-400} = 7.6 \cdot 10^{-6} K^{-1}$ , were measured in the study by Agea-Blanco et al.<sup>[24]</sup> No crystallization during heating could be detected by DTA, as also reported in the study by Agea-Blanco et al.<sup>[24]</sup> for the glass under this study. The coarse glass powder, as received, was crushed in air using a ZrO<sub>2</sub> jaw-crusher (BB51, Retsch, Haan, Germany). To reach an appropriate starting particle size for milling, glass frits were repeatedly crushed, starting with a gap width of 1 mm, which was then decreased in steps of 0.2 mm. The last crushing step (gap width: 0.2 mm) was repeated thrice.

Glass powder milling was conducted in a planetary ball mill (Planetary micro mill pulverisette 7, Fritsch, Idar-Oberstein, Germany) equipped with two 25 mL corundum grinding jars ( $\varnothing_{in} \approx 33$  mm,  $h = 45$  mm), each filled with four corundum balls ( $\varnothing \approx 12$  mm) and  $\approx 8$  g of crushed glass powder. Glass powders were milled for 4 h at maximum motor speed of 3400 r min<sup>-1</sup>. Milling was interrupted every 30 min for 20 min to prevent overheating. Controlled milling in specific atmospheres was facilitated using sealed corundum jars. The sealed jars were evacuated to <10 mbar and refilled with CO<sub>2</sub> (99.99%, Air Liquide, Germany) or Ar (99.99%, Air Liquide, Germany) to  $\approx 1$  bar. Evacuation and gas filling was repeated five times to minimize the amount of residual air. Every 30 min, the atmosphere was renewed following the aforementioned procedure. Milled powders were then stored in a vacuum desiccator at < 2 mbar containing a standard drying agent.

Cylindrical powder compacts were uniaxially pressed at 60 MPa in ambient air ( $\varnothing \approx 5$  mm,  $h \approx 2$  mm,  $m \approx 0.09$  g) without organic additives. Before compaction, milled powders were stored  $\approx 40$  min in high density polyethylene (HDPE) sample boxes in ambient air. Coarse pieces of these compacts were used for VHE degassing studies. Some compacts were heated at 15 K min<sup>-1</sup> to 500 °C and 5 K min<sup>-1</sup> to selected temperatures and quenched in air for electron and laser scanning microscopy (LSM). For XPS, FTIR, and TOF–SIMS studies, these compacts were crushed and re-ground in a metal mortar. For FTIR absorption spectroscopy, KBr pressed pellets were prepared from these powders.

To determine the decomposition temperature range of mechanically damaged small BaCO<sub>3</sub> precipitates, a commercial BaCO<sub>3</sub> powder (Typ A, 99% <45  $\mu$ m, Solvay Barium–Strontium GmbH, Bad-Hönningen, FRG) was 5 min mix-milled with a glass powder of equal mass and similar particle size in ambient air and subsequently studied with DTA. This glass powder was obtained from a jaw-crushed K01 powder by 5 min milling in air prior to mix-milling.

**Methods:** Particle size measurements were carried out using a Mastersizer 2000 (Malvern Instruments, Worcestershire, UK). Prior to each measurement, powders were de-agglomerated by suspending  $\approx 10$  mg of glass powder in a 0.003 M Na<sub>4</sub>P<sub>2</sub>O<sub>7</sub> solution and subsequent treatments for 1–9 min in an ultrasonic bath were conducted. An Autosorb iQ Station 1 (Quantachrome Instruments, Odelzhausen, Germany) was used to measure the Brunauer–Emmett–Teller (BET) surface area. The measuring chamber was outgassed for 3 h at 250 °C prior to the measurement. Krypton 4.0 and Nitrogen 5.0 (Linde, Berlin, Germany) were used for surface area measurements on coarse and fine powders, respectively.

Powders, powder compacts, and bulk glass samples exposed to milling were studied with environmental scanning electron microscopy (ESEM-FEG, Philips-XL 30, Eindhoven, Netherlands) and LSM (OLS4100, Olympus, Hamburg, Germany). Scanning electron microscope (SEM) samples were fixed onto the sample holder using graphite sticks. Prior to imaging, samples were sputter coated with Au.

DTA was conducted in air at 5 K min<sup>-1</sup> (<500 °C at 15 K min<sup>-1</sup>) using  $\approx 25$  mg powder compact fragments in Pt crucibles (TAG 24, Setaram, Caluire, France). The temperature was measured within  $\pm 5$  K accuracy.

Heating microscopy (Leitz, Wetzlar, Germany) with optical data acquisition (Hesse Prüftechnik, Osterode, Germany) was utilized for measuring shrinkage and foaming of cylinder-shaped powder compacts during heating at 5 K min<sup>-1</sup> (<500 °C at 15 K min<sup>-1</sup>) by measuring their silhouette area (shadow image). Results are presented in terms of the powder compact silhouette area change,  $s_A = \Delta A/A_0$ , where  $A_0$  is the silhouette area of the initial (green) powder compact. Temperature accuracy was  $\pm 10$  K.

Gas release from green and sintered powder compacts was studied using VHE combined with mass spectrometer gas detection (QMA4005, Balzers Instruments, Balzers, Liechtenstein). VHE analysis was conducted in vacuum ( $10^{-5}$ – $10^{-7}$  mbar) during heating at 20 K min<sup>-1</sup> using the multiple-ion detection mode. Temperature accuracy was  $\pm 15$  K.

A CS-800 analyzer (Eltra GmbH, Haan, Germany) was used to analyze the total carbon content of glass powders. 15 mg of powder samples were melted by combustion of an iron/tungsten mixture in an oxygen stream. Released carbonaceous species were oxidized to CO<sub>2</sub>, which was then detected by an IR cell.

XPS studies were conducted with an ESCALAB 200X (VG Instruments, East Grinstead, UK). Samples were fixed onto the sample holder using double-sided adhesive polymeric tapes. Measurements were carried out under ultrahigh vacuum with Al K $\alpha$  radiation. The XPS beam typically penetrated up to 10 nm underneath the surface of the sample; the analyzed surface area was  $\approx 10$  mm in diameter. The uncertainty of the measurement of main chemical elements was  $\pm 10\%$  ( $\pm 50\%$  around the detection limit 0.1–1 at.%).

TOF–SIMS measurements were carried out with a TOF–SIMS 4 instrument (ION-TOF, Münster, Germany). Samples were pressed in tin foils, which were mounted on a sample holder using polymer tape, and transferred to the measurement chamber evacuated to  $10^{-10}$  mbar. Analysis was conducted using a pulsed Bi-ion beam in the quasistatic mode (Bi $^{1+}$ , 25 keV @ 0.95 pA). The analyzed surface area was  $\approx 100 \times 100 \mu\text{m}^2$ . Each analysis was repeated eight times. Depth profiles were conducted on coarse glass particles of  $\approx 250$ – $300 \mu\text{m}$  in size by step-wise sputtering and analysis of the eroded area ( $\approx 300 \times 300 \mu\text{m}^2$ ). The sputtering rate was  $\approx 29 \text{ nm min}^{-1}$ . Sputtering was conducted by Cs $^{+}$ -ion bombardment (5 keV @ 51 nA).

Attenuated total reflectance (ATR)–FTIR studies were conducted using an iF6 66v vacuum FTIR spectrometer (Bruker Optik GmbH, Ettlingen, Germany) coupled with an ATR accessory (Diamond Golden Gate) using an HeNe laser emitting 633 nm light at 5 mbar. Powder samples were mechanically fixed onto a diamond substrate by uniaxial pressing. Absorption spectra in the mid-IR were recorded on KBr-pressed pellets containing 2.5 wt% glass powder using a FTIR spectrometer Bruker Vertex 80v. Measurement conditions were globar light source, KBr beam, splitter, and deuterated triglycerine sulfate (DTGS) detector. Typically, 100 scans were accumulated for each spectrum with a spectral resolution of  $2 \text{ cm}^{-1}$ .

## Acknowledgements

The authors gratefully acknowledge experimental support by colleagues I. Feldmann (scanning electron microscope), A. Wagner (X-ray photoelectron spectroscopy), and A. Kohl (attenuated total reflectance accessory–FTIR). The authors finally acknowledge financial support by Erasmus Lifelong Learning Programs for B. Agea-Blanco.

Open access funding enabled and organized by Projekt DEAL.

## Conflict of Interest

The authors declare no conflict of interest.

## Author Contribution

R.M. conducted conceptualization, data curation, project administration, supervision, and visualization. B.A., H.B., S.R., and T.W. conducted the investigation. R.M. and H.B. conducted validation. R.M. and H.B. wrote the original draft. R.M. and H.B. wrote the review and contributed in editing.

## Data Availability Statement

Research data are not shared.

## Keywords

foaming, glass powder, milling, sintering

Published online:

- [1] R. Müller, S. Reinsch, in *Processing Approaches for Ceramics and Composites*, (Eds: N. Bansal, A.R. Boccaccini), John Wiley & Sons: Hoboken, NJ **2012**, p. 75.
- [2] W. A. Schiller, R. Müller, M. Eberstein, S. Reinsch, T. Rabe, *cfi/Berichte der DKG* **2008**, 85, 12.
- [3] E. M. Rabinovich, *J. Mater. Sci.* **1985**, 20, 4259.
- [4] Y. Imanaka, *Multilayered Low Temperature Cofired Ceramics (LTCC) Technology* Springer, New York **2005**.
- [5] M. Lahti, K. Kautio, M. Karppinen, K. Keranen, J. Ollila, P. Karioja, *Int. J. Electron. Telec.* **2020**, 66, 361.
- [6] X. J. Sun, S. S. Yao, J. J. Xing, J. F. Zhang, Y. X. Yang, H. B. Li, H. Tong, X. Yuan, *Mater. Res. Express* **2020**, 7.
- [7] J. Schilm, A. Rost, M. Kusnezoff, S. Megel, A. Michaelis, *Int. J. Appl. Ceram Technol.* **2018**, 15, 239.
- [8] A. De Pablos–Martin, S. Rodriguez–Lopez, M. J. Pascual, *Int. J. Appl. Glass Sci.* **2020**, 11, 552.
- [9] J. König, R. R. Petersen, Y. Z. Yue, *J. Non-Cryst. Solids* **2016**, 447, 190.
- [10] R. R. Petersen, Y. Z. Yue, J. König, *Int. J. Appl. Glass Sci.* **2016**, 7, 524.
- [11] O. V. Suvorova, D. V. Makarov, *Glass Ceram+* **2019**, 76, 188.
- [12] E. Bernardo, H. Elsayed, A. R. Romero, M. C. Crovace, E. D. Zanotto, T. Fey, *Front. Mater.* **2021**, 7.
- [13] J. König, R. R. Petersen, N. Iversen, Y. Z. Yue, *J. Non-Cryst. Solids* **2021**, 553.
- [14] M. H. N. Yio, Y. Xiao, R. Ji, M. Russell, C. Cheeseman, *Ceram. Int.* **2021**, 47, 8697.
- [15] J. J. Zhang, B. Liu, S. E. Zhang, *Sci. Total Environ.* **2021**, 781.
- [16] E. Lucchini, S. Meriani, G. Slokar, *J. Mater. Sci.* **1983**, 18, 1331.
- [17] C. Leonelli, F. Bondioli, P. Veronesi, M. Romagnoli, T. Manfredini, G. C. Pellacani, V. Cannillo, *J. Eur. Ceram. Soc.* **2001**, 21, 785.
- [18] G. H. Hwang, H. J. Jeon, Y. S. Kim, *J. Am. Ceram. Soc.* **2002**, 85, 2956.
- [19] C. Lara, M. J. Pascual, M. O. Prado, A. Duran, *Solid State Ionics* **2004**, 170, 201.
- [20] E. S. Lim, B. S. Kim, J. H. Lee, J. J. Kim, *J. Non-Cryst. Solids* **2006**, 352, 821.
- [21] B. S. Kim, E. S. Lim, J. H. Lee, J. J. Kim, *J. Eur. Ceram. Soc.* **2007**, 27, 819.
- [22] R. Müller, R. Meszaros, B. Peplinski, S. Reinsch, M. Eberstein, W. A. Schiller, J. Deubener, *J. Am. Ceram. Soc.* **2009**, 92, 1703.
- [23] H. R. Fernandes, J. M. F. Ferreira, *J. Eur. Ceram. Soc.* **2007**, 27, 4657.
- [24] B. Agea-Blanco, S. Reinsch, R. Müller, *Front. Mater.* **2016**, 3.
- [25] R. Müller, P. Gottschling, M. Gaber, *Glass Sci. Technol.* **2005**, 78, 76
- [26] G. Liptay, *Atlas of Thermoanalytical Curves* Vol. 5, No. 286, Akademiai Kiado, Budapest, Hungary **1976**.
- [27] C. T. Au, Y. Q. Zhang, H. He, S. Y. Lai, C. F. Ng, *J. Catal.* **1997**, 167, 354.
- [28] S. Maitra, N. Bandyopadhyay, S. Das, A. J. Pal, M. J. Pramanik, *J. Am. Ceram. Soc.* **2007**, 90, 1299.
- [29] A. A. Davydov, *Infrared Spectroscopy of Adsorbed Species on The Surface of Transition Metal Oxides*, (Ed. C. H. Rochester), John Wiley & Sons Ltd, Chichester **1990**.
- [30] E. Stolper, *Geochim. Cosmochim. A.c* **1982**, 46, 2609.
- [31] H. Behrens, A. Stuke, *Glass Sci. Technol.* **2003**, 76, 176.
- [32] C. W. Mandeville, J. D. Webster, M. J. Rutherford, B. E. Taylor, A. Timbal, K. Faure, *Am. Mineral.* **2002**, 87, 813.

Received: April 14, 2021

Revised: June 9, 2021

- [33] R. A. Brooker, S. C. Kohn, J. R. Holloway, P. F. Mcmillan, *Chem. Geol.* **2001**, 174, 241.
- [34] P. L. King, P. F. Mcmillan, G. M. Moore, *Geochem. Explor. Geochem. Remote Sens.* **2004**, 33, 93.
- [35] N. Neuroth, *Glastechnische Berichte* **1968**, 41, 243.
- [36] U. Bauer, H. Behrens, M. Fechtelkord, S. Reinsch, J. Deubener, *J. Non-Cryst. Solids* **2015**, 423, 58.
- [37] C. E. Weir, R. A. Schroeder, *J. Res. Natl. Bureau of Standards – A Phys. Chem.* **1964**, 68A, 465.
- [38] H. Behrens, N. Tamic, F. Holtz, *Am. Mineral.* **2004**, 89, 301.
- [39] H. Behrens, *Chem. Geol.* **2010**, 272, 40.
- [40] *Thermo Scientific XPS: Adventitious Carbon Contamination*, **2017**, <http://xpssimplified.com/elements/carbon.php>.
- [41] L. I. V. M. Haselbach, S. Ma, *Environmental Sci. Technol.* **2008**, 42, 5329.
- [42] A. V. Naumkin, A. Kraut-Vass, S. W. Gaarenstroom, C. J. Powell, *NIST X-Ray Photoelectron Spectroscopy Database* **2012**, <http://srdata.nist.gov/xps/Default.aspx>.
- [43] G. Heinicke, H. P. Hennig, E. Linke, U. Steinike, K. P. Thiessen, K. Meyer, *Tribochemistry* Akademie-Verlag, Berlin **1984**, p. 495.
- [44] R. Baptist, F. Levy, *Vacuum* **1992**, 43, 213.
- [45] E. V. Kalinkina, A. M. Kalinkin, W. Forsling, D. V. Makarov, *Int. J. Miner. Process.* **2001**, 61, 273.
- [46] R. Petrovich, *Geochim. Cosmochim. Ac* **1981**, 45, 1675.
- [47] Y. X. Zhang, H. W. Ni, *Rev. Miner. Geochem.* **2010**, 72, 171.
- [48] W. L. Roumine, A. G. Whittington, P. I. Nabelek, A. M. Hofmeister, *Bull. Vulcanol.* **2012**, 74, 2273.
- [49] H. Behrens, *Rev. Miner. Geochem.* **2010**, 72, 227.
- [50] H. Behrens, Y. X. Zhang, *Earth Planet. Sci. Lett.* **2001**, 192, 363.